AIAA JOURNAL
Vol. 31, No. 1, January 1993

Numerical Prediction of Flap Losses in a Transonic Wind Tunnel

Nide G. C. R. Fico Jr.*
Instituto de Aeronáutica e Espaço, CTA, 12228-904, S. J. dos Campos, SP, Brazil
and
Marcos A. Ortega†
Instituto Tecnológico de Aeronáutica, CTA, 12228-900, S. J. dos Campos, SP, Brazil

Transonic wind-tunnel testing demands mass extraction at the test section. Part of the deviated flow entering the plenum chamber returns to the main stream through flaps that are located upstream of the high-speed diffuser. The main objectives of this paper are to predict values of the flap loss factor and to ascertain the influence of the returning secondary flow on the performance of the high-speed diffuser. As the ultimate goal is to calculate losses, modeling of the physical problem is performed by means of the Navier-Stokes equations. These equations are solved through the use of an implicit finite difference scheme due to Beam and Warming. The flowfield at the flap region, considering the flap as a separate element, is successfully simulated. As a result of the simulation, accurate values of the flap loss factor and of the high-speed diffuser inlet blockage are obtained. Finally, an application related to a practical loss calculation case is performed. It is observed that the flap re-entry flow exerts an important influence on the performance of the high-speed diffuser.

Introduction

THE fundamental problem of the wind-tunnel circuit analysis is to determine the stagnation pressure rise that must be supplied by the main compressor to operate the tunnel at a specified condition at the test section. In other words, the necessary power for maintaining the desired conditions at a tunnel test section is given by the total loss (decrease in availability) along the tunnel circuit. The standard approach for calculating the total loss is to divide the closed circuit into elements and, through one-dimensional analysis, account for each individual element loss.[1,2] By far, the most difficult element to be assessed is the so called "high-speed section" (or "test leg"), which extends from the test-section entrance to the high-speed diffuser entrance. To understand why this particular element is so unique one should bear in mind that several influences have to be accounted for when dealing with it: 1) Reynolds-number deviation from a certain reference condition; 2) presence of the model; 3) presence of the model supporting strut; 4) ventilated walls (slotted or perforated); 5) plenum chamber; 6) second throat; and 7) re-entry flaps. The problem becomes even more severe if one remembers that in an actual wind tunnel run all of those factors come together into the scene.

Faced with the inexistence of individual data for most of these influences, the analyst has to rely on experimental data taken from similar facilities. Usually, static pressure measurements are performed at the entrance of the test section and at the entrance of the high-speed diffuser in such a way that all contributions to the pressure loss factor are lumped into a single coefficient for the whole test leg. The pressure loss coefficient evaluation for the return flaps, treated as a separate element, as well as the influence of such flaps on the high-speed diffuser inlet blockage (consequently on its performance), are the main goals of the present work. Perhaps of all losses the one associated with the re-entry flaps is the most difficult to calculate, due to the interrelation of the main (primary) stream in the tunnel, the secondary stream in the plenum chamber, the returning flow through the flaps, and the action of the auxiliary compressors which control the conditions at the plenum chamber (see Fig. 1).

Received Jan. 17, 1992; revision received May 18, 1992; accepted for publication June 24, 1992.

*Assistant Research Engineer, Transonic Wind Tunnel Development Group (GTTS).

†Professor, Aerodynamics Department. Member AIAA.

As the ultimate motivation of this study is to calculate losses, flowfield simulation must be accomplished by means of the Navier-Stokes equations. To discretize this system of equations, the Beam and Warming implicit finite-difference algorithm[3,4] is called upon. The actual implementation, as applied here, follows much of that presented by Pulliam and Steger,[5] Pulliam,[6] and Azevedo.[7] The time march is performed by means of the implicit Euler method. Although the inviscid terms are discretized by standard second-order central operators, the viscous terms are represented by the so-called midpoint operators. Moreover, the Beam and Warming algorithm is in fact applied to a simplification of the Navier-Stokes equations, known as Reynolds-averaged thin-layer Navier-Stokes equations. To keep the numerical scheme stable, standard fourth-order, constant-coefficient, artificial dissipation terms are added to the explicit operators, whereas second-order ones are introduced into the implicit operators.[8] Boundary-condition implementation is based on the concept of the one-dimensional characteristic relations associated with the inviscid gasdynamic equations. Even though the geometry of the problem is Cartesian, the code developed is written in a general curvilinear system.

In the next section the problem is formulated and the main simplifying hypotheses are introduced. Then the calculation scheme and the boundary conditions are briefly discussed. Following, some aspects of the flow establishment in a transonic wind tunnel, including the so-called optimum suction condition, are briefly reviewed. Finally, the computational results obtained are presented, and a practical application is given.

Basic Formulation

Statement of the Problem

Wind tunnels have to be equipped with ventilated walls to perform tests in the transonic range; this means that part of the flow

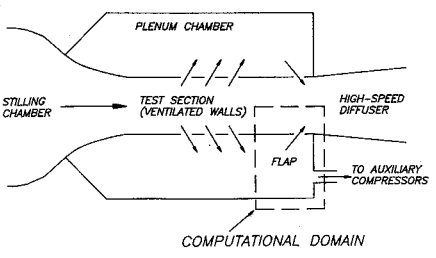

Fig. 1 Sketch of the high-speed section in a transonic wind tunnel.

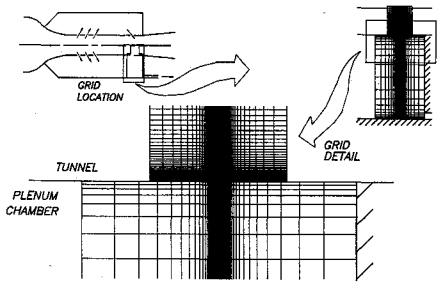

Fig. 2 Computational grid.

entering the test section deviates laterally to the plenum chamber (see Fig. 1). Generally speaking, during normal operation, part of this deviated mass may be evacuated from the plenum chamber by auxiliary compressors, returning to the main stream in a low-speed section of the tunnel. The other part returns through openings in the walls, just ahead of the high-speed diffuser, known as "re-entry flaps." Another common practice is to use only the re-entry flaps to eject mass from the plenum chamber into the main stream at the high-speed diffuser entrance. This is done in tunnels which do not have an auxiliary compressor system or when the auxiliary compressors are turned off. As will be quantified later, this procedure has an adverse effect on the total power requirement of the tunnel.

At this point it is important to define clearly the three types of plenum evacuation this work deals with:

1) *Flap evacuation:* All mass flow leaving the test section through the ventilated walls and entering the plenum chamber returns to the main stream *exclusively* through the re-entry flaps (Fig. 1 without the plenum outlet to the auxiliary compressors).

2) *Mixed evacuation:* Part of the mass flow entering the plenum chamber is evacuated by auxiliary compressors and the remainder by the flaps (Fig. 1).

3) *Compressor evacuation:* All mass flow entering the plenum chamber is evacuated *exclusively* through the auxiliary compressor system (Fig. 1 with the flaps closed).

The use of auxiliary compressors brings about benefits as it diminishes the total power (power of the main compressor plus power of the auxiliary compressors) required to run a transonic wind tunnel.[9] The mixed evacuation is a compromise between the other two types of plenum evacuation as it does not penalize the total power excessively or impose the use of very large auxiliary compressors.

The mixing of the secondary flow through the flaps and the tunnel's primary flow originates the so-called re-entry flap loss. Moreover, the entrainment of these two streams thickens the boundary layer downstream of the flaps. This boundary-layer thickening has another negative consequence, namely, an increase of the blockage factor at the high-speed diffuser entrance. Quantification of those two losses is the principal objective of this work.

The region of the flowfield to be simulated is indicated in Fig. 1. As the interest relies on accounting for the isolated influence of the flaps, the tunnel is considered empty (no model) and the second throat is assumed retracted. The flaps are located one at the floor and the other at the ceiling of the tunnel; they correspond to rectangular openings connecting the tunnel to the plenum chamber (see Fig. 1). The flap length is equal to the distance between the lateral walls, whereas its width is measured along the tunnel's longitudinal direction. In general, the flap width is much smaller than its length—their ratio being of order 10^{-1}. Hence, tip effects may be neglected and the flowfield can be considered as approximately two dimensional. Furthermore, the whole physical situation is considered to be symmetrical relative to the horizontal central plane of the tunnel.

Numerical Scheme, Turbulence Model, and Boundary Conditions

The Reynolds-averaged thin-layer Navier-Stokes equations written in conservation-law form for a body-conforming, two-dimensional, curvilinear coordinate system are solved in this work. The Beam and Warming implicit approximate factorization algorithm[3] is used and the actual implementation follows closely the works of Pulliam and Steger,[5] and Pulliam.[6] The reader should refer to these authors for more details.

Turbulence closure is accomplished by means of the two-layer eddy-viscosity Baldwin and Lomax model.[10] Applying the Baldwin and Lomax scheme to this problem brings in a point of concern: this closure model was originally developed for wall boundary layers, however, the flap represents a gap in the wall. A justification is due, and therefore the following arguments are invoked. First, the flap width is small when compared to a characteristic tunnel length. Second, the outflow through the flaps is a very small fraction of the tunnel mass flow (see the "Results and Discussion" section). Thus, when passing by the flap, the boundary layer developing along the wall "feels" just a small bump. It is true that there is an incipient separation before the gap, but right after it the boundary layer reattaches. The fact is that the main stream, including here the boundary layer, is mildly disturbed by the mass outflow through the flap. This assures the applicability of the Baldwin and Lomax turbulence closure model. Moreover, this reasoning also justifies the thin-layer assumption that is incorporated into the problem modeling. The turbulent Prandtl number Pr_t is taken to be constant and equal to 0.9. In reality, this parameter varies throughout the boundary layer. However, if the molecular Prandtl number value Pr is close to unity (which is the case for air), Pr_t is practically constant within the boundary layer.[11]

Figures 1 and 2 show the computational domain. It is located at the flap influence zone and covers both the main tunnel stream and the plenum chamber. At all entrance and exit planes (test section and plenum domains), boundary-condition enforcement is based on the one-dimensional characteristic relations of the inviscid gasdynamic equations. The basic concept is that the Euler equations can be diagonalized by a similarity transformation.[12] Then, one-dimensional characteristic relations can be derived which represent the propagation of flow information along characteristic lines. At the walls, considered adiabatic, the no-slip condition is applied and the pressure follows the "boundary-layer assumption," $p_{1,j} = p_{2,j}$ (the "level 1" representing the wall). Because of the problem symmetry, only the flowfield lower half was used to form the computational domain. To facilitate the enforcement of the symmetry boundary conditions, the midplane is located at the grid level $j = j_{\max}-1$, where $j_{\max}$ is the total number of points in the η direction (normal to the wall). Furthermore, the so-called implicit boundary conditions were implemented to render the algorithm more robust.

In terms of boundary conditions, the most important aspect of this particular problem is the exchange of information that takes place at the flap opening. Taking a look at Fig. 1, one can see that there is a wall inside the computational domain, and that the gap in this wall, providing communication between the two sides, represents the re-entry flap. This situation leads to a two-grid problem, one of them representing the tunnel and the other the plenum chamber; see Fig. 2. Therefore, the numerical solution alternates between the two grids. When the problem is being solved for the tunnel, the boundary condition at the flap opening, whose points are common to both grids, is given by the re-entry velocity distribution corresponding to the last available solution for the plenum chamber. When the problem is being solved for the plenum chamber, the flap opening represents a subsonic exit boundary condition

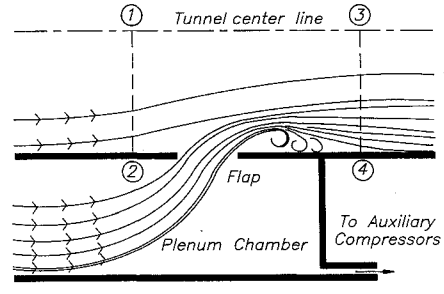

Fig. 3 Re-entry flap influence region. Planes 1–2 and 3–4 limit the flap-influence zone.

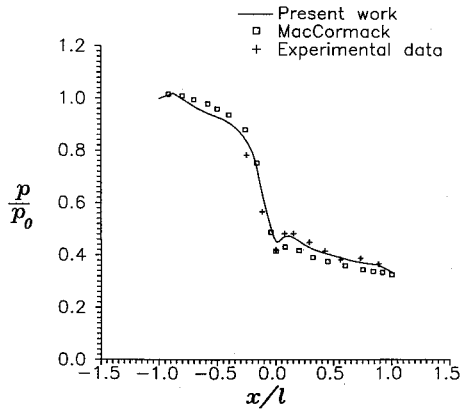

Fig. 4 Static pressure distribution at a transonic convergent-divergent nozzle wall.

where the pressure distribution is fixed by the last available solution at the tunnel.

Another very important aspect deserves to be mentioned. For a specified setting of the tunnel, for which the plenum evacuation is done by the mixed process, the total mass flow being evacuated (therefore crossing the plenum inlet plane) and the mass flow that crosses the flap opening is mostly determined by the auxiliary compressors. The exact amount of those flows has to be properly simulated by the numerical procedure. This is done by varying the pressure at the exit of the plenum chamber which corresponds to the auxiliary compressors inlet (see Fig. 1). This can be recognized as an overall "constraining condition" to the problem as a whole, and represents an extra difficulty to the calculation. One has to run the code several times until the proper balance of mass flows is satisfied.

As seen in Fig. 2, a convenient exponential stretching was introduced to cluster grid points near the flap opening and solid walls. The basic characteristics of the two grids used are 1) points in the ξ direction (streamwise direction): 71 for the tunnel and 56 for the plenum; 2) points in the η direction (transverse direction): 50 for the tunnel and 21 for the plenum; 3) the stretching factor for the tunnel in the ξ direction is 1.25 and in the h direction is 1.075; for the plenum these values are 1.30 and 1.40 in the ξ and η directions, respectively; 4) on both sides, in a region that extends from one flap width upstream of the flap leading edge to one flap width downstream of the flap trailing edge no ξ-direction stretching was used; 5) for the various cases treated in this research, the y^+ value of the first point off the wall varied from 6 (just inside the viscous sublayer[13]) to about 15 (well inside the buffer zone[13]); this y^+ variation was due, primarily, to the Mach number. Although it may be argued that a grid refinement study is desirable, this was out of the authors' possibilities due to the lack of computational power. However, one should keep in mind the integral aspect of the problem which, in a sense, minimizes the importance of the details of the boundary-layer structure. Further, it should be mentioned that the results obtained in this work are in good agreement with the experimental data available, as will become clear in the discussions to come.

Flap Loss Factor K_F

This describes how the flap loss factor K_F was determined after the flowfield numerical solution was obtained. As the process is considered adiabatic, the loss at the flap is directly related to the stagnation pressure drop Δp_0, which in turn is directly associated with the entropy variation of the flow passing through the flap region. After the numerical calculation is completely converged, any desired flow property at any grid point can be calculated. Then, it is possible to determine the entropy at grid points located on two planes normal to the tunnel's walls. These two planes are chosen so as to limit the flap influence zone (see Fig. 3). Knowing entropy values at those planes, and also knowing the mass flow crossing them, it is possible to determine the mean value of the entropy at the inlet and at the exit boundaries. Having determined the mean entropy variation $\Delta\tilde{s}$, the ratio of "mean" stagnation pressure

$$\tilde{p}_{0_e}/\tilde{p}_{0_i} = \exp(-\Delta\tilde{s}/R) \tag{1}$$

can be obtained. The subscript i denotes the inlet plane (plane 1–2 of Fig. 3), whereas the subscript e denotes the exit plane (plane 3–4 of Fig. 3). R stands for the gas constant. Equation (1) can be solved for $\tilde{p}_{0_e}$ and finally K_F is obtained by

$$K_F = \Delta\tilde{p}_0/q = (\tilde{p}_{0_i} - \tilde{p}_{0_e})/q \tag{2}$$

where q is the inlet dynamic pressure.

Diffuser Blockage Factor B_t

For the two-dimensional case, the expression for the blockage factor becomes[14]

$$B_t = 2\delta^*/W \tag{3}$$

where δ^* is the boundary-layer displacement thickness and W the diffuser height, both taken at the diffuser entrance plane.

Code Validation

Before attempting to calculate the flowfield at the flap region, the computational code had to be validated. This was achieved through the simulation of several well-established physical situations of increasing complexity. These are the laminar Couette flow, the pressure driven laminar flow between two parallel plates, the turbulent Fanno flow, the turbulent transonic flow through a two-dimensional convergent-divergent nozzle, and finally the interaction of a shock wave and a laminar boundary layer. For the sake of conciseness, only the last two will be discussed here.

Figure 4 provides comparison among present results, numerical results due to MacCormack,[15] and experimental data by Mason et al.,[16] for the transonic nozzle. The position $x/l = 0$ corresponds to the nozzle geometric throat. Upstream of the throat, both numerical solutions present deviations when compared to the experimental data. In spite of this the present scheme tends to follow the experimental data more closely, especially at the beginning of the contraction. Downstream of the throat, present results fit the experimental data much better. It is important to mention that the numerical scheme proposed here is second-order accurate in space while MacCormack's scheme is only first-order accurate.

Because of the integral aspect of the flap loss coefficient calculation, a very important result is shown in Fig. 5. This figure reproduces the flowfield due to the interaction of a shock wave with a laminar boundary layer. The calculated pressure field recovers all of the main physical aspects of this complex situation, especially those related to the nature (compression and expansion) and positioning of the waves. The figure is drawn to scale, and the wave angles are being reproduced with very good accuracy. Moreover, the dimensionless value of the static pressure obtained for the region after the wave system, i. e., $p = 1.40$, coincides with the experimental value (see Hakkinen et al.[17]). Figure 6 compares the velocity profiles at the separation region. Plotted data correspond to present work, MacCormack,[18] and Hakkinen et al.[17] As can be observed, present results follow the same general trend as MacCormack's data but are closer to the experimental values.

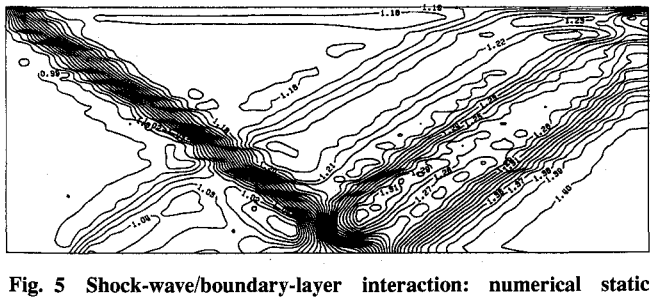

Fig. 5 Shock-wave/boundary-layer interaction: numerical static pressure field.

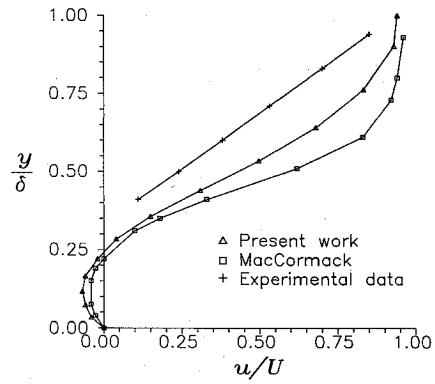

Fig. 6 Shock-wave/boundary-layer interaction: velocity profiles at the position where the wave reaches the wall, u is the local velocity, U the freestream velocity, y the distance from the wall, and δ the boundary-layer thickness.

Transonic Wind-Tunnel Flow Establishment

Continuous Mach-number variation can be obtained in a transonic wind tunnel by using either a simple sonic nozzle or a multijack flexible Laval nozzle. In the case of a sonic nozzle, the set Mach number is varied by adding suction to the plenum chamber surrounding the test section walls. Thus, the required ratio between test section and throat cross-sectional areas is simulated by mass flow removal. As the necessity for test section mass extraction is greater for sonic nozzles than it is for convergent-divergent ones, the practical upper Mach-number limit in the former case is about 1.3. Beyond this value, the amount of test section mass extraction needed for the use of a sonic nozzle increases very rapidly, prohibiting its use.

For a fixed nozzle-test section configuration (i.e., fixed nozzle setting, test section wall angle, and diffuser re-entry flap position), the test section Mach number M_{TS} is established according to a curve defined by the relationship between the main compressor pressure ratio λ_c and the plenum chamber suction $\dot{m}_s/\dot{m}$ (Pindzola[19]). Here $\dot{m}_s$ is the extracted mass flow and $\dot{m}$ represents the mass flow at the test section entrance. Although a set Mach number can be attained using different values of this relationship, only a single combination of these parameters exists such that the test section flow is fully established and the diffuser entrance flow is not overexpanded. This condition is called the "optimum pressure ratio-suction setting" (or simply "optimum suction").

Figure 7 (from Ref. 19) shows the effects of operating at other than the optimum suction setting. The general trend for both subsonic and supersonic regimes is similar, therefore only the subsonic case ($M_{TS} = 0.85$) will be discussed in detail. Points related to the various diffuser entry Mach numbers are marked a through g. The point marked e, for which M_{TS} is uniform along the test section, represents the optimum suction. An increase in suction beyond this point results in a decrease in Mach number at stations just upstream of the diffuser entrance. On the other hand, a decrease in suction below this point first results in an increase in Mach number at the rear of the test section up to point c at which the diffuser entrance is choked, and then in an overexpansion in the diffuser entrance as the pressure ratio is further increased.

One must keep in mind that the total power associated to the optimum point can be reduced if more mass is extracted from the test section into the plenum chamber, but, as a penalty, the uniform-flow testing length would be diminished accordingly.

Results and Discussion

Some Aspects of the Flowfield

In the transonic range the mass flow through the re-entry flaps is usually small. Therefore the main stream is mildly disturbed in a very restricted region adjacent to the flaps. To demonstrate the robustness of the numerical algorithm and also to ascertain the physical scenario of the flowfield in the flap mixing region, a preliminary case which presents a much more pronounced influence

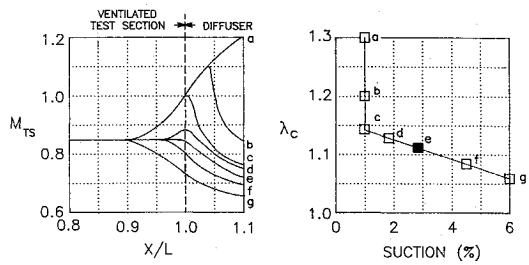

Fig. 7 Optimum suction definition.

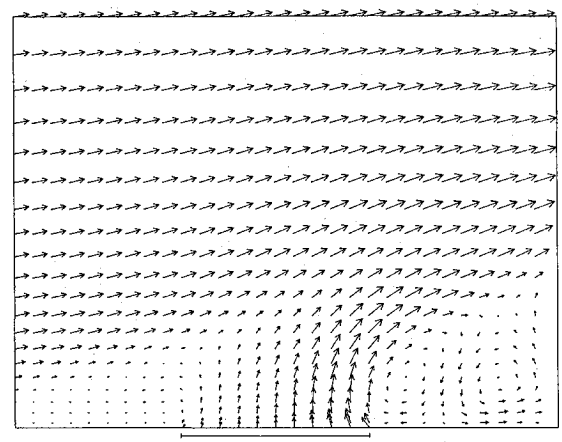

Fig. 8 Velocity field of the primary stream at the flap vicinity for M_{TS} = 0.3. The horizontal bar indicates the flap opening.

of the secondary flow on the primary one was simulated. The test section Mach number M_{TS} was chosen to be 0.3. The ratio of secondary flow to main flow is 1.6% and flap evacuation is used. Even though this situation has no practical application for wind tunnels (there is no need to extract mass from the test section at such a low value of M_{TS}), it is a very illustrative one. The velocity vector field in the mixing region is plotted in Fig. 8. One can observe boundary-layer separation before the flaps and a great recirculation zone after them—as physically expected.

Flowfield details for a case at the transonic range are now presented. Figures 9 and 10 show the pressure level curves in the flap vicinity for $M_{TS} = 0.9$ with the re-entry flaps closed and opened, respectively. By observing those figures, the reader can appreciate the blockage imposed by the flap outflow on the tunnel's primary stream and the consequent effect on the pressure field. This influence is basically what will be quantified next.

Selected Cases

In the course of this investigation, various tunnel settings were simulated to assess the various flow-establishment alternatives that were just reviewed briefly. Table 1 lists the seven different situations studied. The Mach numbers ranged from 0.9 to 1.2, the types of nozzle were used, and the plenum chamber evacuation procedure was also varied. Each case will now be referred to by its number as it appears on Table 1. The principal reasoning behind the cases' selection is the optimum suction concept.

Next, the numerical simulation results for all of the preceding selected cases are presented and discussed. Emphasis is given to the calculated values of the flap loss factor and of the high-speed diffuser blockage, which are the primary objectives of this study.

Test Section Mach-Number Influence—Cases 1–4

In these four situations the test section Mach number varies from 0.9 to 1.2. The difference in nozzle types (see Table 1) is a direct consequence of the usual operational practice of transonic wind tunnels. In all cases, the plenum evacuation used is of the mixed type and the mass flow extracted from the test section represents 2.7% of the tunnel total mass flow[19] (optimum suction). As already mentioned, the mixed evacuation returns only part of the

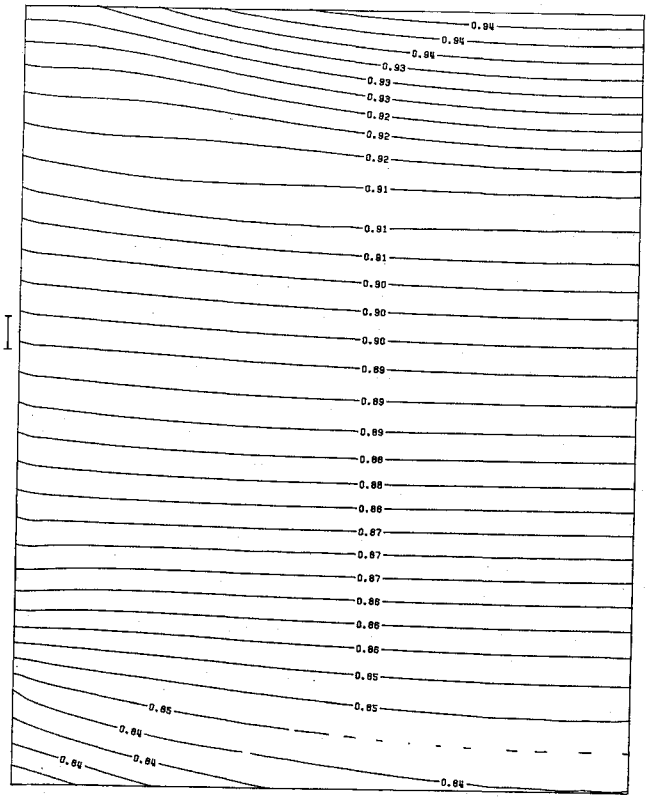

Fig. 9 Static pressure level curves for the primary stream in the vicinity of the closed flap for M_{TS} = 0.9. The horizontal bar indicates the flap position.

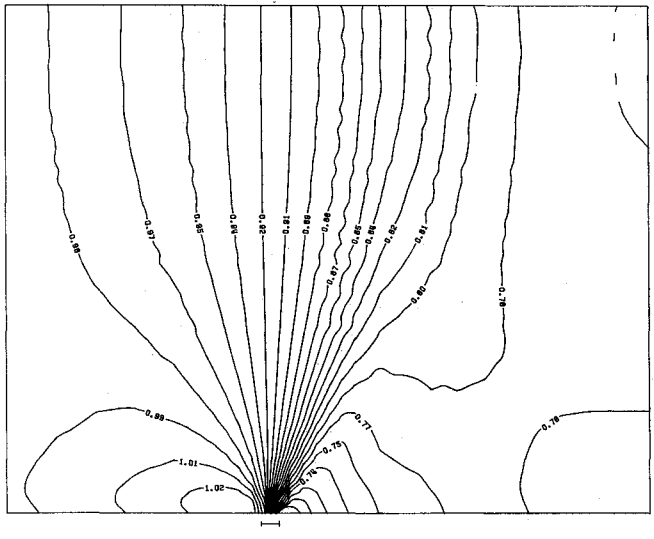

Fig. 10 Static pressure level curves for the primary stream in the vicinity of the opened flap for M_{TS} = 0.9. The horizontal bar indicates the flap opening.

extracted test-section mass through the flaps. Figure 11 displays the behavior of the flap loss coefficient K_F as a function of the test section Mach number M_{TS}. As M_{TS} increases, the secondary flow through the flap disturbs the primary flow of the tunnel with diminishing intensity, and consequently the value of K_F is inversely proportional to M_{TS}. Physically, this is in agreement with what one would expect: as the velocity of the main flow increases, so does its momentum, becoming ever more difficult for the secondary flow to influence it. For M_{TS} = 0.9, the secondary flow through the flaps is only 0.7% of the mass flow at the test-section entrance; for M_{TS} = 1.2 this number decreases to 0.06%. A curve fitting of the results for cases 1–4 gives the following equation for K_F in the Mach number range investigated:

$$K_F = 2.1485 - 5.6708M_{TS} + 4.9950M_{TS}^2 - 1.4667M_{TS}^3 \qquad 0.9 \le M_{TS} \le 1.2 \tag{4}$$

Figure 12 shows how the re-entry mass flow affects the high-speed diffuser inlet blockage. The flow conditions are exactly the same as above. As expected, the blockage factor B_t becomes larger as one opens the flaps. These higher values of B_t will penalize the diffuser performance, causing an additional loss due to the re-entry flaps. This effect is seldom (if ever) taken into account in tunnel loss calculations due to the complete lack of information. In this respect, Fig. 12 is a helpful tool in determining the influence of the flaps on the high-speed diffuser performance.

Evacuation-Type Influence

Cases 2 and 5

As already mentioned, there are different ways to evacuate the plenum chamber. Two of them (flap evacuation and mixed evacuation) are related to mass flow through the re-entry flaps, and are, therefore, of interest to the present simulation. For a fixed value of test section mass extraction, the entropy variation associated to flap evacuation is of course greater than the one related to mixed evacuation. Therefore both K_F and B_t will attain higher values if the tunnel operates with flap evacuation of the plenum chamber. Table 2 shows, among other results, the evacuation-type influence for M_{TS} = 1.0. In Table 2, $\dot{m}$ is the mass flow at the test section entrance, $\dot{m}_s$ is the extracted mass flow, and $\dot{m}_F$ is the mass flow through the flaps.

Cases 4 and 6

The evacuation type is evaluated for Lava/nozzle at M_{TS} =1.2. The results appear in Table 2. As can be seen in the table, the values of K_F and B_t are much greater for the case of flap evacuation. This explanation is found in the last column of Table 2. The outflows through the flaps is greater when flap evacuation is used. Greater outfolows correspond to greater disturbances in the main stream.

Nozzle Type Influence

Cases 4 and 7

Since the sonic nozzle demands more test section mass extraction, it is bound to generate a higher flap loss because the secondary stream through the flaps is "stronger" than the one for the Laval nozzle. The numerical results quantifying how the nozzle type influences K_F and B_t, for M_{TS} = 1.2, are also shown in Table 2. It is apparent from Table 2 that 1) use of a sonic nozzle demands

Table 1 Selected cases

Mach number	Nozzle type	Evacuation type: Flap	Evacuation type: Mixed
0.9	Sonic		(1)
1.0	Sonic	5	(2)
1.1	Laval		(3)
1.2	Laval	6	(4)
1.2	Sonic		(7)

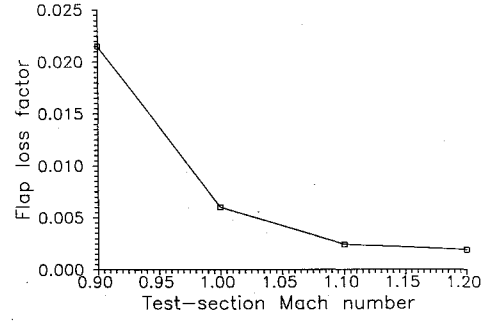

Fig. 11 K_F as a function of M_{TS}; mixed evacuation.

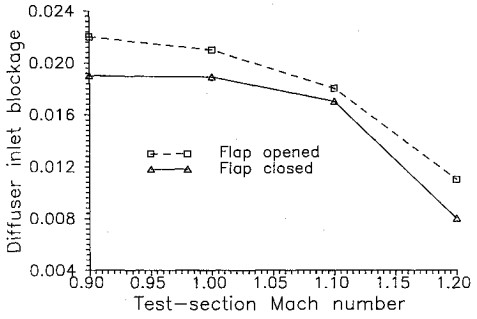

Fig. 12 Influence of the re-entry flap secondary flow on the high-speed diffuser blockage B_t; mixed evacuation.

Table 2 Results for different cases

Case	K_F	B_t	$\dot{m}_s/\dot{m}$	$\dot{m}_F/\dot{m}$
2	6.00×10^{-3}	2.10×10^{-2}	0.027	0.0190
4	1.89×10^{-3}	1.10×10^{-2}	0.027	0.0006
5	1.60×10^{-2}	4.60×10^{-2}	0.027	0.0270
6	1.25×10^{-2}	5.20×10^{-2}	0.027	0.0270
7	5.21×10^{-3}	2.93×10^{-2}	0.075	0.0009

must more mass extraction, and 2) for both nozzles the plenum evacuation mechanism is of the mixed type $[(\dot{m}_F/\dot{m}_s < (\dot{m}_s/\dot{m})]$. Furthermore, $\dot{m}_F/\dot{m}$ is greater for the case of the sonic nozzle. Hence, one identifies immediately two disadvantages of sonic nozzle operation: greater values of K_F and B_t, and more power consumption by the auxiliary compressors.

Circuit Loss: Re-Entry Flap as a Separate Element

Up to this point, the values of the coefficients K_F and B_t for several situations have been presented. However, these numbers do not mean much by themselves. It is important to apply these results to a circuit-loss calculation to take full advantage of the numerical simulation. For this purpose case number 5 was selected, mainly because it is possible to compare it with existing data.

The circuit-loss calculation was performed in a typical transonic wind tunnel. The test section flow conditions are Mach number $M_{TS} = 1.0$, stagnation pressure $p_0 = 101$ KPa, and stagnation temperature $T_0 = 313$ K. The test section geometric characteristics are height = 2.0 m, width = 2.4 m, and length = 8.5 m. The plenum chamber height is 6.0 m. The average distance between the flap centerline and the high-speed diffuser entrance is 1.15 m. The tunnel is divided into elements which are marked by numbers (see Fig. 13).

Figure 14, a very useful plot to wind-tunnel designers, shows the loss percentage of every tunnel element. The usual one-dimensional pressure loss calculation scheme[1,2] was used to come up with the results presented in Fig. 14. There are, however, two major differences: the flap is treated as a separate element and its influence on the high-speed diffuser, due to the increase of B_t, is quantified—using for that the results of this work. These two aspects are not usually taken into account by existing approaches of wind tunnel pressure loss determination. Taking a closer look at Fig. 14, it is possible, for example, to appreciate the degradation of the high-speed diffuser performance. Originally, this element contributes to 20% of the circuit total loss, but as the flaps open this value increases to about 30%. This result confirms that flap evacuation, even in small amounts, penalizes to a great extent the high-speed diffuser performance.

The loss at the re-entry flaps, calculated with the results of the flowfield numerical simulation, is about 5% of the total circuit loss (see Fig. 14). Experimental results[9] for the Boeing pilot wind tunnel with $M_{TS} = 1.25$, the same type of plenum evacuation considered here and with four re-entry flaps (our model accounts for only two), show that 7.3% of that tunnel's total loss is due to the flaps. The Boeing pilot facility has a different number of flaps and was run at a different test section Mach number. This case was taken as

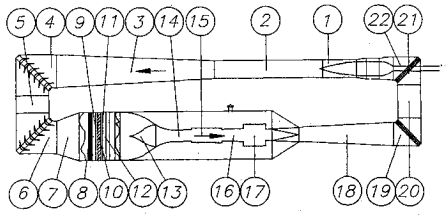

Fig. 13 Sketch of the various elements of a transonic wind tunnel.

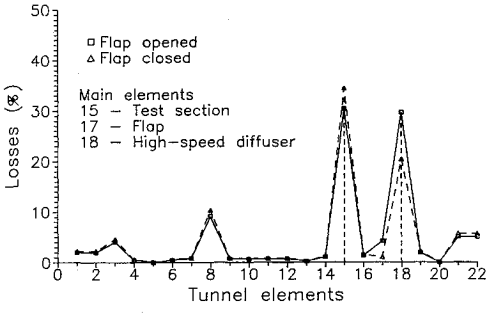

Fig. 14 Pressure loss percentage distribution.

reference due to the scarcity of available experimental data. Notwithstanding this, comparison of those two values—5.0 and 7.3%—demonstrates the reliableness of the present numerical simulation.

Concluding Remarks

The flowfield at the re-entry flap region of a transonic wind-tunnel test section has been successfully predicted. The finite difference computer code developed, with special attention to the boundary conditions, to solve the Reynolds-averaged thin-layer Navier-Stokes equations has proven to be an efficient and robust procedure for simulating the main physical phenomena, especially the thickening of the boundary layer occurring downstream of the flap opening. As a result of the simulation, quantification of the flap loss factor and of the influence of the flaps on the high-speed diffuser entrance blockage was accurately performed. It was then observed that the influence of the secondary stream through the flaps on the high-speed diffuser performance is appreciable. These data are of paramount importance to transonic wind-tunnel designers and analysts.

References

[1]Stich, P. B., "Mathematical Modeling of the AEDC Propulsion Wind Tunnel (16T)," Arnold Engineering Development Center, AEDC TR-84-32, Arnold Air Force Station, Tullahoma, TN, March 1985.

[2]Eckert, W. T., Mort, K. W., and Jope, J., "Aerodynamic Design Guidelines and Computer Program for Estimation of Subsonic Wind Tunnel Performance," NASA TD-N-8243, Oct. 1976.

[3]Beam, R. M., and Warming, R. F., "An Implicit Factored Scheme for the Compressible Navier-Stokes Equations," *AIAA Journal*, Vol. 16, No. 4, 1978, pp. 393–402.

[4]Warming, R. F., and Beam, R. M., "On the Construction and Application of Implicit Factored Schemes for Conservation Laws," *SIAM-AMS Proceedings*, Vol. 11, 1978, pp. 85–129.

[5]Pulliam, T. H., and Steger, J. L., "Implicit Finite-Difference Simulations of Three-Dimensional Compressible Flow," *AIAA Journal*, Vol. 18, No. 2, 1980, pp. 159–167.

[6]Pulliam, T. H., "Euler and Thin Layer Navier-Stokes Codes: ARC2D, ARC3D," Notes for Computational Fluid Dynamics User's Workshop, The Univ. of Tennessee Space Institute, Tullahoma, TN, March 1984.

[7]Azevedo, J. L. F., "Transonic Aeroelastic Analysis of Launch Vehicle Configuration," Ph. D. Dissertation, Dept. of Aeronautics and Astronautics, Stanford Univ., Stanford, CA, Feb. 1988 (also available as NASA CR-4186, Oct. 1988).

[8]Pulliam, T. H., "Artificial Dissipation Models for the Euler Equations," *AIAA Journal*, Vol. 24, No. 12, 1986, pp. 1931–1940.

[9]Goethert, B. H., *Transonic Wind Tunnel Testing*, Pergamon Press, Oxford, 1961, pp. 356–380.

[10]Baldwin, B. S., and Lomax, H., "Thin Layer Approximation and

Algebraic Model for Separated Turbulent Flows," AIAA Paper 78-257, Jan. 1978.

[11]Cebeci, T., and Bradshaw, P., *Physical and Computational Aspects of Convective Heat Transfer,* Springer-Verlag, New York, 1984, pp. 152–153.

[12]Warming, R. F., Beam, R. M., and Hyett B. J., "Diagonalization and Simultaneous Symmetrization of the Gas-Dynamic Matrices," *Mathematics of Computation,* Vol. 29, No. 132, 1975, pp. 1037–1045.

[13]Anderson, D. A., Tannehill J. C., and Pletcher, R. H., *Computational Fluid Mechanics and Heat Transfer,* McGraw-Hill, New York, 1984, pp. 224.

[14]Ghose, S., and Kline, S. J., "The Computation of the Optimum Pressure Recovery in Two-Dimensional Diffusers," *Journal of Fluids Engineering,* Vol. 100, Dec. 1978, pp. 419–426.

[15]MacCormack, R. W., "Current Status of Numerical Solutions of the Navier-Stokes Equations," AIAA Paper 85-0032, Jan. 1985.

[16]Mason, M. L., Putnam, L. E., and Re, R. J., "The Effect of Throat Contouring on Two-Dimensional Converging-Diverging Nozzles at Sonic Conditions," NASA TP-1704, 1980.

[17]Hakkinen, R. J., Greber, I., Trilling, L., and Abarbanel, S. S., "The Interaction of an Oblique Shock Wave with a Laminar Boundary Layer," NASA Memo 2-18-59w, March 1959.

[18]MacCormack, R. W., "A Numerical Method for Solving the Equations of Compressible Viscous Flow," AIAA Paper 81-0110, Jan. 1981.

[19]Pindzola, M., "Transonic Wind Tunnels," *Lecture Notes in Transonic Aerodynamics,* The Univ. of Tennessee Space Institute, Tullahoma, TN, March 1984, pp. 10–18.